Earth Syst. Sci. Data Discuss., doi:10.5194/essd-2016-27, 2016
Manuscript under review for journal Earth Syst. Sci. Data
Published: 22 July 2016

Open Access Earth System Science Data Discussions

An Extended Global Earth System Data Record on Daily Landscape Freeze-Thaw Status Determined from Satellite Passive Microwave Remote Sensing

Youngwook Kim[1,*], John S. Kimball[1], Joseph Glassy[2], and Jinyang Du[1]

[1]Numerical Terradynamic Simulation Group, College of Forestry & Conservation, The University of Montana, Missoula, MT 59812

[2]Lupine Logic, Inc., Missoula, MT 59802

[*]Corresponding Author: youngwook.kim@ntsg.umt.edu

For Submission to: *Earth System Science Data*

Earth Syst. Sci. Data Discuss., doi:10.5194/essd-2016-27, 2016
Manuscript under review for journal Earth Syst. Sci. Data
Published: 22 July 2016

Abstract

The landscape freeze-thaw (FT) signal determined from satellite microwave brightness temperature (T_b) observations has been widely used to define frozen temperature controls on land surface water mobility and ecological processes. Calibrated 37 GHz T_b retrievals from the Scanning Multichannel Microwave Radiometer (SMMR), Special Sensor Microwave Imager (SSM/I), and SSM/I Sounder (SSMIS) were used to produce a consistent and continuous global daily data record of landscape FT status at 25-km grid cell resolution. The resulting FT Earth System Data Record (FT-ESDR) is derived from a refined classification algorithm and extends over a larger domain and longer period (1979-2014) than prior FT-ESDR releases. The global domain encompasses all land areas affected by seasonal frozen temperatures, including urban, snow-ice dominant and barren land. The FT retrieval is obtained using a modified seasonal threshold algorithm (MSTA) that classifies daily T_b variations in relation to grid cell-wise FT thresholds calibrated using surface air temperature data from model reanalysis. The resulting FT record shows mean annual spatial classification accuracies of 90.3 and 84.3 percent for PM and AM overpass retrievals relative to global weather station measurements. Detailed data quality metrics are derived characterizing effects of sub-grid scale open water and terrain heterogeneity, and algorithm uncertainties on FT classification accuracy. The FT-ESDR results are also verified against other independent cryospheric data, including *in situ* lake and river ice phenology, and satellite observations of Greenland surface melt. The expanded FT-ESDR enables new investigations encompassing snow and ice dominant land areas, while the longer record and favorable accuracy allow for refined global change assessments that can better distinguish transient weather extremes, landscape phenological shifts, and climate anomalies from longer-

Earth Syst. Sci. Data Discuss., doi:10.5194/essd-2016-27, 2016
Manuscript under review for journal Earth Syst. Sci. Data
Published: 22 July 2016

Open Access Earth System Science Data Discussions

term trends extending over multiple decades. The data set is freely available online (http://dx.doi.org/10.5067/MEASURES/CRYOSPHERE/nsidc-0477.003).

Earth Syst. Sci. Data Discuss., doi:10.5194/essd-2016-27, 2016
Manuscript under review for journal Earth Syst. Sci. Data
Published: 22 July 2016

1. Introduction

The freeze-thaw (FT) signal detected from moderate frequency (37 GHz) satellite microwave brightness temperature (T_b) observations is sensitive to changes in the relative abundance of liquid water at the land surface between frozen and non-frozen conditions. The FT metric defines the predominant landscape frozen or non-frozen status within a sensor footprint and is insensitive to potential degradation from solar illumination variations and atmosphere cloud/aerosol contamination effects. These properties enable consistent global coverage and daily monitoring from available satellite microwave sensors (Kim et al., 2011; Zhao et al., 2014). Global satellite microwave sensors have been operational since the mid-1970's, while similar T_b observations from overlapping sensor records have enabled the development of one of the longest satellite environmental data records, delineating global daily FT dynamics and associated climate trends over multiple decades (Kim et al. 2011). The FT Earth System Data Record (FT-ESDR) was developed to provide a consistent and continuous long-term daily global FT data record to support climate, ecological and hydrological application studies. The initial FT-ESDR domain encompassed global vegetated land areas where seasonal frozen temperatures are estimated to be a significant constraint to annual vegetation growth. The FT retrieval is derived on a grid-cell-wise basis using a temporal change classification of similar daily 37 GHz T_b observations from Scanning Multichannel Microwave Radiometer (SMMR), Special Sensor Microwave Imager (SSM/I) and SSM/I Sounder (SSMIS) sensor series, in relation to frozen and non-frozen T_b reference states.

The FT-ESDR has been widely used to define frozen temperature constraints to ecological and hydrological processes, and for monitoring seasonal shifts in land surface energy partitioning where frozen temperatures are a significant part of the annual cycle (Mao et al., 2015; Zhang et al, 2014; Zhu et al., 2016). Previous FT-ESDR applications have included documenting widespread increases in the annual thaw cycle and relaxing frozen temperature constraints to vegetation growth over the Northern Hemisphere from regional climate warming (Kim et al. 2012; Wang et al., 2015); analyzing spring thaw and frost related impacts on vegetation phenology and productivity (Buermann et al. 2013; Kim et al. 2014b); and defining a potential growing season climate indicator for the US National Climate Assessment (Kenney et al., 2014). The FT-ESDR has also been used to document FT related impacts to surface hydrology, including evapotranspiration and the timing and extent of seasonal snowmelt (Zhang et al. 2011; Kim et al. 2015), and river ice phenology (Park et al. 2016b). The FT-ESDR defined frozen season was also used to estimate recent changes in permafrost extent and stability over the pan-Arctic (Park et al., 2016a).

In this investigation, we utilize calibrated daily (AM and PM overpass) 37 GHz T_b retrievals from SMMR, SSM/I and SSMIS sensor series to refine and extend the FT-ESDR. New FT-ESDR enhancements include a larger global domain encompassing all land areas affected by seasonally frozen temperatures, including vegetated, barren, urban, ice and snow cover dominant, and open water inundated areas. We exploit continuing SSM/I operations to develop a longer data record (1979-2014) than prior FT-ESDR releases (Kim et al., 2014c). A modified seasonal threshold algorithm (MSTA) is used to classify daily FT status in relation to a T_b based FT threshold calibrated annually for each grid cell using daily surface air temperature (SAT) records from global model reanalysis. The FT classification accuracy is evaluated using independent daily SAT measurements from the global weather station network. Annual quality assessment (QA) maps are derived using empirical models describing estimated global variations in FT classification accuracy due to climate and terrain heterogeneity, open water cover and model calibration uncertainty. The FT-ESDR performance is also evaluated using other cryosphere data records including *in situ* lake and river ice phenology observations and satellite derived Greenland surface melt dynamics. The FT-ESDR methods, database description and performance assessment are provided in the following sections.

2. Data and methods

2.1. Satellite microwave brightness temperature observations

The Nimbus-7 SMMR Pathfinder dataset contains T_b retrievals from October 1978 to August 1987. The SSM/I and SSMIS sensor records are part of the Defense Meteorological Satellite Program (DMSP) platform series and provide continuous global, twice-daily T_b measurements from August 1987 to the present. The SMMR sensor obtained T_b retrievals at multiple frequencies (6.6, 10.7, 18.0, 21.0, and 37.0 GHz), with vertical (V-) and horizontal (H-) polarizations (pol). The SMMR T_b measurements were obtained at a constant 50.31° incidence angle and noon, and midnight equatorial crossings (i.e., overpass times). The SSM/I and SSMIS sensors obtain V- and H-pol T_b measurements at 19.3, 37.0 and 85.5 GHz, and 22.2 GHz T_b measurements at V-pol only. The SSM/I and SSMIS instruments have a constant 53.1° measurement incidence angle and approximate 6AM/PM equatorial crossings.

Calibrated, overlapping 37 (V-pol) GHz T_b data records used for classifying FT status were acquired from SMMR (Knowles et al., 2000), SSM/I and SSMIS (Armstrong et al., 1994) in a consistent 25 km grid cell resolution global Equal-Area Scalable Earth Grid (EASE-Grid) v1.0 projection format (Brodzik and Knowles, 2002). Missing T_b data composed approximately 34.3±24.3 [inter-annual SD] percent of frozen temperature affected land areas on an annual basis for the 1979-2014 record. Missing T_b data attributed to orbital gaps between satellite overpasses, particularly for the mid-latitudes, were filled on a grid cell-wise basis by linear interpolation of temporally adjacent, successful T_b retrievals to generate spatially and temporally consistent daily (AM and PM overpass) T_b observations as inputs for the landscape FT classification following previously established methods (Kim et al., 2011). The SMMR record was matched to the SSM/I record using pixel-wise adjustment of the SMMR T_b record based on empirical analyses of overlapping SMMR and SSM/I T_b measurements for 1987 to ensure cross-sensor consistency (Kim et al., 2012). Large temporal T_b gaps in January and December 1987 and January 1988 were filled using empirical relationships developed from ERA-Interim (Dee et al, 2011) global model reanalysis SAT and satellite T_b data records. The resulting daily T_b record used to construct the FT-ESDR extended over a 36- year period (1979 to 2014).

The 37 GHz T_b retrievals used in the FT-ESDR have relatively high atmospheric transmittance and are sensitive to land surface FT conditions (Andre et al., 2015; Holmes et al., 2013); the V-pol T_b retrievals used in the FT-ESDR are also relatively less sensitive to soil moisture variation, snow and ice stratification, and scattering than the H-pol retrievals (Green et al., 2012; Homes et al., 2009; Owe et al., 2008). The 37 GHz T_b sensitivity to landscape FT variations from surface soil, snow cover and vegetation elements within the sensor footprint is related to a relatively shallower characteristic microwave emitting depth than lower frequency T_b retrievals (Green et al., 2012), while the 37 GHz emitting depth is generally greater under drier surface conditions (Ulaby and Long, 2014).

2.2. Global FT-ESDR domain

We used quarter-degree resolution ERA-Interim daily minimum SAT (SAT_{min}) estimates and a simple cold temperature constraint index to define the global FT-ESDR domain as all land areas where seasonally frozen temperatures influence ecological processes and land surface water mobility (Kim et al. 2011). The ERA-Interim global reanalysis was selected for the FT-ESDR domain definition, because it contains consistent atmospheric and surface analyses with similar spatial and temporal resolution as the satellite T_b records. The 36-year (1979-2014) quarter-degree ERA-Interim daily SAT_{min} global record was resampled to a 25 km global EASE-Grid format. A cold temperature constraint index, CCI [days yr^{-1}], was derived for each global EASE-Grid cell using a bioclimatic growing season index and SAT_{min} as developed in Kim et al. 2011. The CCI values were derived for each year of the 36-year ERA-Interim record on a per grid cell basis and used to identify cells constrained by seasonal frozen temperatures. The FT-ESDR domain was defined where the CCI exceeded a minimum threshold (5 days yr^{-1}) from the 36-year average CCI record following previously developed methods (Kim et al., 2011). The prior FT-ESDR domain included only vegetated land areas where frozen temperatures are a major constraint to ecological processes, while the new FT-ESDR domain described in the current investigation is 41.5 percent (~27 million km^2) larger and encompasses all frozen temperature affected land areas, including vegetated, urban, open water, snow-ice dominant, and barren landscapes.

2.3. Freeze-thaw algorithms

A Modified Seasonal Threshold Algorithm (MSTA) was used to classify daily (AM and PM) FT status from calibrated, overlapping 37 GHz (V-pol) T_b time series from SMMR, SSM/I and SSMIS records. The MSTA algorithm is defined as:

$$\text{FT status} = \begin{cases} Non-frozen, & if\ Tb > threshold \\ Frozen, & if\ Tb \le threshold \end{cases} \quad (1)$$

Earth Syst. Sci. Data Discuss., doi:10.5194/essd-2016-27, 2016
Manuscript under review for journal Earth Syst. Sci. Data
Published: 22 July 2016

The MSTA FT threshold was defined annually using an empirical linear regression relationship between the satellite T_b retrievals and daily ERA-Interim SAT estimates established for each grid cell. The FT thresholds were derived separately for the satellite T_b time series from AM and PM overpasses and using corresponding daily SAT minimum (SAT_{min}) and maximum (SAT_{max}) values. The ERA-Interim SAT record was selected for calibrating the FT algorithms, because FT-ESDR derived from ERA-Interim reference states produced the best FT classification accuracy relative to alternative reference states defined from other model reanalysis datasets and satellite (MODIS) land surface temperature (LST) records (not shown). Larger weighting of SAT values closer to 0°C was used in selecting the corresponding T_b based FT threshold for each grid cell; weighting of the SAT and T_b regression relationship was derived using a cosine function within a temperature range extending from -60.0°C to 30.0°C and representing 99 percent of the SAT frequency distribution defined from the 36-year ERA-Interim SAT global climatology. The MSTA algorithm assumes that the large changes in microwave dielectric constant of the land surface that occur around the 0°C temperature threshold are associated with landscape FT transitions that dominate the corresponding satellite 37 GHz T_b seasonal dynamics, rather than other potential sources of T_b variability (Kim et al., 2011). An advantage of the MSTA relative to an earlier seasonal threshold algorithm (STA) based FT classification (Kim et al. 2011) is that the T_b threshold selection does not depend on frozen and non-frozen reference states derived by averaging T_b measurements over respective winter and summer periods, and is less sensitive to T_b data gaps during these reference periods. The resulting AM and PM FT classifications were combined into a daily composite (CO) with four discrete classification levels, including frozen (AM and PM frozen), non-frozen (AM and PM non-frozen), transitional (AM frozen; PM thawed), and inverse-transitional (AM thawed; PM frozen) states.

Earth Syst. Sci. Data Discuss., doi:10.5194/essd-2016-27, 2016
Manuscript under review for journal Earth Syst. Sci. Data
Published: 22 July 2016

2.4. FT classification agreement and quality assurance

We used independent *in situ* daily SAT_{min} and SAT_{max} measurements from the global weather station network to assess the FT classification agreement following previously developed methods (Kim et al., 2011, 2012). The WMO weather station daily SAT measurements were obtained from the National Climate Data Center (NCDC) Global Summary of the Day (NWS, 1988). The Euclidian distance between each FT-ESDR EASE-Grid cell centroid and WMO station locations was computed to select a single representative station closest to the center of a grid cell when two or more stations were located within the same EASE-Grid cell. Daily SAT_{min} and SAT_{max} records for the selected stations were used to define daily frozen ($T \leq 0$°C) and non-frozen ($T > 0$ °C) temperature conditions and compared with corresponding FT classification results from the overlying EASE-Grid cells and respective AM and PM overpass periods, assuming that the local timing of daily SAT_{min} and SAT_{max} occurs near the satellite equatorial crossing times (Frolking et al., 1999; Kim et al., 2012). The FT classification agreement was assessed through grid cell-to-point comparisons between WMO daily SAT measurements and overlying FT-ESDR based FT results. Previous studies indicate close correspondence between the SAT and 37 GHz (V-pol) FT dynamics (Kim et al., 2011, 2012), which characterize the FT state of the topmost surface layer within a 25-km satellite footprint, including bare soil, snow, and vegetation elements (Owe and Van De Griend, 2001). Approximately 4153±632 [inter-annual SD] weather stations were selected for the 1979-2014 period. Differences between the SAT measurement based FT value and FT-ESDR based FT estimate from the overlying grid cell were used to define the global daily FT spatial classification accuracy, expressed as a proportion (%) of the number of stations and overlying FT-ESDR grid

Earth Syst. Sci. Data Discuss., doi:10.5194/essd-2016-27, 2016
Manuscript under review for journal Earth Syst. Sci. Data
Published: 22 July 2016

cells with identical FT classification results relative to the total WMO station cells represented within the FT-ESDR domain on an annual, monthly and daily basis.

The mean annual FT classification agreement between WMO station SAT observations and FT-ESDR classification values was evaluated according to the dominant land cover characteristics within a grid cell, sub-grid scale terrain heterogeneity and open water body fraction within a grid cell, and other factors potentially influencing FT classification agreement. The MODIS (MCD12C1, collection 051) 5.6-km, 17-class IGBP yearly global land cover product for the 2001-2012 MODIS record (Friedl et al., 2010) was used to define dominant land cover categories within each 25-km resolution FT-ESDR grid cell using a majority approach (de Jong et al., 2013; Dendoncker et al., 2008). A 300-m water body map for the 2010 epoch (from 2008 to 2012) produced from European Space Agency (Defourny et al., 2016) was used to derive fractional open water coverage (F_w, %) within each 25-km FT-ESDR grid cell. A 1-km resolution digital elevation model (DEM; Hasting et al., 1999) was used to derive an elevation gradient (m), defined as the spatial standard deviation (SD) of the elevation distribution within each 25-km FT-ESDR grid cell. Drop-in-bucket averaging of finer resolution (300-m and 1-km) pixels was used to resample to the 25-km resolution EASE-Grid format.

A FT-ESDR Quality Assurance (QA) map was determined on an annual basis from multivariate linear regression analysis of global annual FT classification agreement with WMO weather station based FT results and four independent geospatial variables. The independent variables used in the QA analysis for each grid cell included the F_w, elevation gradient, mean annual duration of transitional FT conditions, and the correlation (r-value) between weighted ERA-Interim reanalysis SAT and satellite T_b time series used to define the MSTA FT threshold. The resulting QA calculations defined the mean annual classification accuracy (%) for each grid cell and year of record, and were linearly rescaled between low (0) and best (1) relative quality values to define a final dimensionless QA metric. Quality Control (QC) flags were used to identify other potential factors affecting FT classification agreement, including grid cells and days with missing and interpolated T_b observations, and grid cells characterized by extensive open water bodies ($F_w > 0.2$), complex terrain (elevation gradient > 300m), and precipitation events (Ferraro et al., 1996).

2.5. Comparison of FT metrics with independent Cryosphere data records

Three FT metrics were derived from the daily CO FT classification series for each year of record, including frozen season (FS) duration, primary spring thaw date, and non-frozen season (NFS) duration. The FS duration was defined from the daily FT-ESDR as the total number of frozen or transitional (AM frozen, PM non-frozen) days per year (September-August), which is similar to number of frost days reported by Peterson, (2005). The primary spring thaw date was determined as the first day (DOY) when 12 out of 15 consecutive days from January through June were classified as non-frozen (Kim et al., 2012). The NFS was defined as the number of classified non-frozen days for a calendar year (January- December). The resulting FT metrics were compared against other independent cryospheric data records, including lake and river ice duration observations from the Global Lake and River Ice Phenology Database from 1979 to 2013 (Benson and Magnuson, 2000); reported annual ice breakup dates for the Tanana river in the interior of Alaska (Nenana Ice Classic, 2011); and the NASA MEaSUREs Greenland surface melt record (Mote, 2014). The annual duration of lake and river ice was determined for each observation location as the period between reported seasonal freezing and thawing and compared with collocated FT-ESDR based FS estimates. The reported Tanana river ice breakup dates from

Earth Syst. Sci. Data Discuss., doi:10.5194/essd-2016-27, 2016
Manuscript under review for journal Earth Syst. Sci. Data
Published: 22 July 2016

1979 to 2003 were compared against the FT-ESDR defined mean primary spring thaw dates for the surrounding basin defined within the overlying 5x5 grid cell (~15,625 km^2) window. The NASA MEaSUREs Greenland surface melt records were available from 1979 to 2012 at the time of this investigation and were compared against corresponding FT-ESDR derived annual NFS results. The Greenland surface melt records distinguish two categorical surface conditions, including surface melt and no surface melt. The seasonal progression in proportional area and annual variation of surface melt and FT-ESDR NFS conditions were derived over the Greenland ice sheet area indicated from the Land-Ocean-Coastline-Ice database (Knowles, 2004).

3. Results

3.1. Global FT-ESDR domain and frozen season characteristics

The resulting FT-ESDR domain represents ~60.5% (~93 million km^2) of the global land area, compared to ~52.5% for prior FT-ESDR releases (Kim et al., 2011). The larger FT-ESDR domain encompasses vegetation, urban, large water body (F_w < 100%), snow-ice-dominant, high mountain, and barren land areas (Figure 1). The maps in Figure 1 show the mean annual frozen season (FS) and FS temporal SD derived from the 36-year (1979-2014) FT-ESDR record. The FS duration is approximately 151±82 [spatial SD] days and 201±167 days for respective Northern Hemisphere (NH) and Southern Hemisphere (SH) domains. The FT-ESDR captures characteristic FS increases at higher elevations, including Tibetan Plateau, Andes and Rocky Mountain areas, though finer spatial scale FT variations over complex terrain are less distinct due to the coarse (25-km) resolution T_b retrievals. The FT-ESDR also depicts characteristic FS increases at higher latitudes, with maximum FS durations over polar permanent ice and snow areas of Greenland and Antarctica. The FS is generally shorter along coastal margins relative to

Earth Syst. Sci. Data Discuss., doi:10.5194/essd-2016-27, 2016
Manuscript under review for journal Earth Syst. Sci. Data
Published: 22 July 2016

inland areas, consistent with more moderate maritime climate conditions in the coastal zone. Annual FS variability is generally greater along the zones of transition between major air masses and associated climate regimes. Higher FS variability is also evident for coastal grid cells and equatorial climate zones, which may reflect greater FT classification uncertainty in these areas as indicated from the FT classification and quality assessments described below.

3.2. FT classification assessment

The mean annual FT spatial classification agreement over the global FT-ESDR domain and derived from the 36-year calibrated SMMR, SSM/I and SSMIS T_b record was 90.3±1.4 [inter-annual SD] percent and 84.3±1.7 [inter-annual SD] percent for respective PM and AM overpasses (Figure 2) as derived from daily grid cell-to-point comparisons against *in situ* SAT measurement based FT observations from 4153±632 [inter-annual SD] global WMO weather stations. The FT classification results show positive trends ($p<0.001$) toward increasing mean annual classification agreement of 1.4 and 1.1 percent per decade for respective AM and PM overpasses over the 1979-2014 record. The increase FT accuracy coincides with a 0.3°C/decade mean SAT warming trend over the FT-ESDR domain and may be due to a corresponding decline in frozen conditions (Kim et al., 2012). The apparent FT accuracy trend may also reflect differences between SMMR and SSM/I portions of record, including variations in the location and number of weather stations used for validation and different overpass times between SMMR (noon/midnight) and SSM/I (~6PM/AM) T_b records. The lower FT classification agreement from the AM overpass T_b record is attributed to generally cooler diurnal temperature conditions and a corresponding larger number of daily FT variations over the annual cycle in the AM record relative to characteristic warmer mid-day temperature conditions and fewer FT variations in the

Earth Syst. Sci. Data Discuss., doi:10.5194/essd-2016-27, 2016
Manuscript under review for journal Earth Syst. Sci. Data
Published: 22 July 2016

PM results. Lower AM FT classification agreement may also be due to wetter surface conditions and temperature inversions during night-time diurnal SAT minimums (Owe and Van De Griend, 2001).

Monthly mean FT classification agreement for AM and PM overpasses and the 1979-2014 record are summarized in Table 1 for global, NH and SH domains. The FT classification agreement was assessed using daily SAT measurements from approximately 3912±556 and 241±102 respective NH and SH weather stations for the 1979-2014 record. The monthly pattern of mean FT classification agreement is generally lowest and highest for corresponding NH winter frozen and summer non-frozen seasons. Similarly, the monthly pattern for AM overpass FT results show larger agreement in summer relative to winter in the SH, while the monthly agreement pattern for PM overpass results in the SH is more consistent throughout the year. Generally warmer temperatures and fewer frozen days in the SH promote higher and more temporally consistent FT classification agreement in the PM overpass record relative to the NH.

The mean annual FT spatial classification agreement from the PM overpass results in relation to 5344 global WMO station observations for a selected year (2012) is 92.4±9.9 [spatial SD] percent (Figure 3). Lower latitude areas with characteristic warmer temperatures show generally greater mean annual FT classification agreement due to a longer non-frozen period. Relatively lower agreement occurs along coastal margins, and in mountainous regions and high elevation areas. Sub-grid scale heterogeneity in microwave dielectric properties and associated FT conditions within the coarse (25-km Res.) satellite footprint increase FT classification uncertainty along coastal margins (Howell et al., 2009; Kimball et al., 2001). In mountainous regions, complex terrain and microclimate variability promote heterogeneous frozen and non-frozen conditions within the coarser resolution satellite footprint leading to greater FT classification uncertainty (Du et al., 2015). Arid climate areas with dry land surface conditions (e.g. Tibetan Plateau) have a deeper characteristic microwave emitting depth and larger volume scattering relative to areas with wetter surface conditions (Prigent et al., 2006; Han et al., 2015); these conditions may promote a lower FT signal-to-noise and lower classification agreement with WMO SAT measurements (Grody and Basist, 1996; Han et al., 2015).

The FT-ESDR classification daily error matrices for 2012 AM and PM overpasses were assessed relative to corresponding WMO SAT defined FT dynamics (Figure 4). Mean global daily FT classification agreement is generally lower during seasonal FT transitions and highest during the predominantly non-frozen summer season. Spatially and temporally heterogeneous SAT and FT conditions promote lower FT classification agreement during seasonal transition periods (Du et al. 2015, Kim et al. 2011). Two cases of FT classification disagreement between the satellite and *in situ* measurements include: WMO thaw/FT-ESDR Freeze and WMO Freeze/FT-ESDR Thaw. The WMO Freeze/FT-ESDR Thaw category implies earlier FT-ESDR spring thaw and later fall freeze relative to the WMO FT results, whereas a reverse pattern is observed for the WMO thaw/FT-ESDR Freeze category. The results of the FT classification error matrices suggest a mixture of both freeze and thaw classification errors during the seasonal transition periods.

The mean annual FT classification agreement for the selected year (2012) is summarized in Table 2 for different land cover categories. Grid cells dominated by open water bodies show the lowest FT classification agreement consistent with previous studies (Derksen et al., 2005; Du et al., 2015; Lemmetyinen et al., 2011); however, the FT-ESDR results still show favorable agreement for water affected grid cells despite expected larger constraints from T_b noise effects due to surface dielectric variations and microwave scattering over open water bodies. Permanent

Earth Syst. Sci. Data Discuss., doi:10.5194/essd-2016-27, 2016
Manuscript under review for journal Earth Syst. Sci. Data
Published: 22 July 2016

snow and ice dominant grid cells also show generally lower FT agreement than the other land cover classes, which may be due to variable surface scattering effects on 37 GHz microwave emissions over snow and ice (Chang et al., 1990; Matzler, 1994); the apparent FT classification accuracy is still favorable in these areas, but is based on relatively sparse WMO station observations. For most land cover classes the PM FT classification agreement is generally greater than the AM overpass results except for snow and ice dominant grid cells where the AM FT classification agreement is approximately 2% greater than the PM overpass results; the greater apparent AM accuracy is attributed to a lower number of FT variations for AM than PM overpasses over relatively cold, snow and ice dominant land areas throughout the year.

3.4. Factors affecting FT classification agreement

The FT-ESDR results determined from the 37 GHz T_b retrievals are sensitive to the predominant frozen or non-frozen status of the land surface within the sensor footprint. However, the actual FT pattern may be spatially complex due to variations in microclimate and land cover conditions that may not be adequately resolved by the coarse (~25 km resolution) satellite sensor footprint (Colliander et al., 2012; Du et al., 2015). The relative agreement between the FT-ESDR and *in situ* station based FT results is therefore expected to be inversely proportional to land surface heterogeneity, including open water abundance and terrain complexity within the grid cell.

We investigated potential factors influencing FT classification agreement between the FT-ESDR and WMO SAT observations, including the open water fraction (F_w, %) and elevation gradient (m) within 25-km resolution EASE-grid cells coinciding with the WMO validation stations. We also examined other factors potentially affecting FT classification agreement

Earth Syst. Sci. Data Discuss., doi:10.5194/essd-2016-27, 2016
Manuscript under review for journal Earth Syst. Sci. Data
Published: 22 July 2016

including the level of per grid cell correspondence (r-value) between the T_b retrievals and weighted ERA-Interim daily SAT estimates used in determining the MSTA FT threshold (Eq. 1), and the mean annual number of classified transitional FT days defined from AM and PM overpass T_b retrievals.

The mean annual FT classification agreement was analyzed for the selected year (2012) and found to be inversely proportional to F_w (slope=-0.25%, $p<0.001$) as shown in Figure 5a. These results confirm generally strong sensitivity of the 37 GHz T_b observations to the presence of surface water within the satellite footprint. The T_b sensitivity to F_w is consistent with large differences in dielectric properties, scattering albedo and microwave emissions between open water and adjacent land areas (Lemmetyinen et al., 2011; Rees et al., 2006). The T_b over lake ice may also be elevated relative to adjacent land areas during the frozen season (Green et al., 2012). These factors contribute to a general mismatch between *in situ* SAT observations that predominantly reflect local land surface conditions and satellite sensor T_b retrievals representing an integrated regional signal.

The FT classification agreement was inversely proportional to the elevation gradient (slope=-0.01%, $p<0.001$) within a grid cell (Figure 5b), but with less apparent impact than F_w. This negative relationship is consistent with generally greater heterogeneity in landscape dielectric properties and FT patterns, and associated microclimate variability in complex terrain, which may not be effectively delineated by the coarse (25-km) grid cell resolution (Du et al., 2015; Podest et al., 2014).

The FT classification agreement was directly proportional to the mean correlation between the satellite T_b retrievals and weighted ERA-Interim SAT used to define the MSTA FT threshold for each grid cell (slope=34.3%; $p<0.001$; Figure 5c). These results indicate that the FT classification is strongly sensitive to the reliability of estimated T_b threshold values, which may be influenced by uncertainty associated with use of reanalysis temperature data (Alexeev et al., 2012; Han et al., 2015; Screen et al., 2012). However, there were relatively few validation stations in cells with larger F_w cover, complex terrain, or lower T_b and SAT correlations, which may contribute uncertainties in assessing the impacts of these factors on FT classification accuracy.

The mean annual FT classification agreement was generally lower for grid cells with a longer FT transitional season (slope=-0.1%, $p<0.001$; Figure 5d). These results are consistent with generally greater FT spatial heterogeneity and reduced classification agreement during seasonal transition periods (Figure 4). These results are also consistent with previous studies documenting increased FT spatial complexity during seasonal transitions in spring and fall (Du et al., 2015; Naeimi et al., 2012; Rautiainen et al., 2014).

3.5. FT quality assurance assessment

The global QA map provides a discrete, grid cell-wise indicator of relative FT-ESDR quality that accounts for potential negative impacts from F_w cover, terrain complexity, length of FT transitional season, and MSTA FT threshold uncertainty influencing mean annual classification accuracy. The resulting annual QA map for selected year 2012 is presented in Figure 6 and shows regions of relative high to low quality. The QA values were stratified into a smaller set of discrete categories ranging from low (estimated mean annual FT classification agreement < 70%) to best (> 95%) quality. Mean proportions of the four QA categories encompass 54.1% (best), 36.0% (good; 85-95% agreement), 6.6% (moderate; 75-85% agreement), and 3.3% (low) of the global FT-ESDR domain. The QA based multivariate regressions were computed on an annual

Earth Syst. Sci. Data Discuss., doi:10.5194/essd-2016-27, 2016
Manuscript under review for journal Earth Syst. Sci. Data
Published: 22 July 2016

basis and explained more than half (56.9±0.04 [inter-annual SD] percent) of the observed global variation in mean annual FT classification agreement (R^2) with the global WMO SAT validation stations over the 1979-2014 record.

The FT-ESDR contains additional quality control (QC) flags that identify other factors potentially affecting FT classification accuracy. The QC flags are spatially and temporally dynamic, and assigned on a per grid cell basis to denote missing satellite T_b records that are subsequently gap-filled through temporal interpolation of adjacent T_b retrievals prior to the FT classification. The QC flags also distinguish grid cells with large open water areas (F_w>0.20) and extreme elevation gradients (>300m), and days with large precipitation events. The FT estimates are derived for open water dominated grid cells allowing greater FT coverage, including extensive boreal and arctic wetland areas that were screened from previous FT-ESDR releases (Kim et al. 2011), while the F_w dominant cells are assigned a QC flag indicating lower expected FT classification accuracy in these areas. Thus, daily FT estimates are still produced for grid cells with gap-filled T_b values, large F_w cover, extreme elevation gradients and large precipitation events, but with dynamic QC flags indicating potentially lower data quality (e.g. Fig. 5).

3.6. FT-ESDR metrics comparison against independent Cryosphere data

3.6.1. Lake and river ice phenology

The FT-ESDR based mean annual FS metric was directly proportional to annual ice duration observations (r=0.938; p<0.001) from the Global Lake and River Ice Phenology Database (1979-2013) as summarized in Figure 7. The observed annual mean ice duration anomalies are obtained from 183±133.8 [inter-annual SD] stations and locations representing northern (≥36°N) land

Earth Syst. Sci. Data Discuss., doi:10.5194/essd-2016-27, 2016
Manuscript under review for journal Earth Syst. Sci. Data
Published: 22 July 2016

areas. These results indicate a direct frozen season impact on lake and river ice phenology, where years with a relatively longer (shorter) FS coincide with extended (reduced) ice duration. The FT-ESDR generally captures the observed annual lake and river ice variations despite lower apparent FT classification agreement in F_w affected areas (Figure 5).

The FT-ESDR defined primary spring thaw date metric also showed favorable correspondence (r=0.79; p<0.01) with observed annual variations in spring Ice breakup for the Tanana River (64.56°N, 149.09°W) in interior Alaska over the 1979-2003 observation record (Figure 8); here, *in situ* river ice breakup date measurements on the lower Tanana river are compared with the average FT-ESDR primary spring thaw date within a 5x5 grid cell domain centered over the site. Years with relatively early (late) river ice breakup in spring correspond with generally early (late) FT-ESDR defined spring thaw onset. The 37 GHz T_b retrievals and FT-ESDR results are largely sensitive to the onset of seasonal snowmelt within the basin, which increases runoff and the spring flood pulse that determine river ice breakup timing (Park et al. 2016b; Rawlins et al. 2005). However, other factors influence lake and river ice phenology, including snow cover depth, ice thickness, water temperature and wind, which may contribute to differences between the satellite and *in situ* measurements.

3.6.2. Greenland surface melt season

The seasonal progression in the proportional area of surface melt (Mote, 2014) and FT-ESDR derived non-frozen conditions over the Greenland ice sheet is shown for the selected year (2012) in Figure 9a. Both daily records show similar seasonal patterns, but with the spring increase in non-frozen conditions preceding the onset of surface melt. The FT-ESDR results also show a 4.3 percent larger non-frozen area relative to active melt areas. The FT-ESDR derived mean annual

NFS over Greenland for 2012 is 50.1±29.1 [spatial-SD] days (Figure 9b), with a shorter NFS for inland areas. The FT-ESDR also shows an extended NFS over the Greenland ice sheet in 1987, 1991, 2002 and 2012, relative to the long-term (1979-2014) satellite record (Figure 9c). The extended NFS years are consistent with observed annual surface melt extremes documented from previous studies (Abdalati and Steffen, 2001; Hakkinen et al., 2014; Nghiem et al., 2012). The FT-ESDR annual mean NFS variability is directly proportional to annual mean surface melt area anomalies for Greenland over the 1979-2012 record ($r=0.535$; $p<0.001$; Figure 9c). Both the FT-ESDR and Greenland surface melt data show generally increasing trends in NFS (1.7 days decade^{-1}; $p=0.2$) and annual melt area (0.03 million km^2 decade^{-1}; $p<0.001$). These results coincide with a 0.6°C decade^{-1} ($p<0.01$) regional SAT warming trend indicated from the ERA-Interim reanalysis.

4. Summary and conclusions

A new FT-ESDR was developed encompassing a larger global domain, longer (1979-2014) data record and refined classification algorithms relative to prior FT-ESDR versions (Kim et al. 2011). The FT-ESDR results show generally favorable agreement with daily FT estimates defined from global WMO weather station SAT measurements; the FT classification agreement was generally stronger for vegetated land areas (mean annual spatial accuracy from 77-97% for AM and PM overpasses), but was also favorable where other land cover classes were dominant within a grid cell, including urban (89.5-96.4%), barren land (91.8-94.3%), water bodies (75.0-77.5%) and snow and ice covered areas (81.1-83.1%). The FT-ESDR results also showed general consistency with a broad set of other cryosphere datasets, including global lake and river ice phenology observations, and Greenland surface melt cycles.

Earth Syst. Sci. Data Discuss., doi:10.5194/essd-2016-27, 2016
Manuscript under review for journal Earth Syst. Sci. Data
Published: 22 July 2016

Open Access Earth System Science Data Discussions

The mean annual FT spatial classification accuracy relative to WMO weather station SAT measurements was approximately 90.3% (PM overpass) and 84.3% (AM overpass) over the global FT-ESDR domain and a 36-year satellite record. The apparent FT classification agreement was generally lower for grid cells with larger F_w cover, greater elevation complexity, and longer FT transitional periods. The FT classification agreement was also directly proportional to the correlation between the satellite T_b retrievals and corresponding ERA Interim global reanalysis based SAT values used for grid cell-wise calibration of MSTA FT thresholds. These results were used to define a relative FT-ESDR annual QA metric that explained more than half of the observed global variability in mean annual FT classification agreement. However, the grid cell-to-point comparisons used for the QA assessment contained relatively few stations in cells with extreme terrain or F_w conditions, or with large disagreement between satellite and *in situ* FT dynamics, which lead to potential uncertainties in the FT classification assessment. Other factors potentially affecting FT classification accuracy were represented by dynamic QC flags assigned on a daily basis for each affected grid cell.

Overall, the expanded global domain and generally favorable FT-ESDR performance enables new potential science investigations encompassing wetlands, mountains and snow/ice dominant land areas that were excluded from earlier FT-ESDR versions. The longer FT-ESDR also enables more refined assessments of global environmental changes that distinguish transient weather extremes, landscape phenological shifts and periodic climate anomalies from longer-term climate trends extending over multiple decades.

Dataset availability

The FT-ESDR is archived and distributed by the NASA National Snow and Ice Data Center Distributed Active Archive Center (NSIDC DAAC). The FT-ESDR can be downloaded from the NSIDC data server (http://nsidc.org/data/nsidc-0477).

Acknowledgements

This work was conducted at the University of Montana under contract to NASA, & supported under the NASA Making Earth System data records for Use in Research Environments (MEaSUREs) program (NNX14AB20A).

Earth Syst. Sci. Data Discuss., doi:10.5194/essd-2016-27, 2016
Manuscript under review for journal Earth Syst. Sci. Data
Published: 22 July 2016

Open Access Earth System Science Data Discussions

References

Abdalati, W., and K. Steffen. (2001). Greenland ice sheet melt extent: 1979-1999. *Journal of Geophysical Research*, 106 (D24), 33983-33988

Alexeev, V. A., I. Esau, I. V. Polyakov, S. J. Byam, and S. Sorokina. (2012). Vertical structure of recent arctic warming from observed data and reanalysis products. *Climate Change*, 111, 215-239

Andre, C., C. Ottle, A. Royer, and F. Maignan. (2015). Land surface temperature retrieval over circumpolar Arctic using SSM/I-SSMIS and MODIS data. *Remote Sensing of Environment*, 162, 1-10

Armstrong, R., K. Knowles, M. Brodzik, and M.A. Hardman. (1994). updated 2015. DMSP SSM/I-SSMIS Pathfinder Daily EASE-Grid Brightness Temperatures. Version 2 [1987-2014]. Boulder, Colorado USA: NASA DAAC at the National Snow and Ice Data Center (http://nsidc.org/data/nsidc-0032.html)

Benson, B. and J. Magnuson. (2000). updated 2012. Global Lake and River Ice Phenology Database. [indicate subset used]. Boulder, Colorado USA: National Snow and Ice Data Center. http://dx.doi.org/10.7265/N5W66HP8

Brodzik, M. J., and K. W. Knowles. (2002). EASE-Grid: A versatile set of equal area projections and grids in Discrete Global Grids, M. Goodchild, Ed. Santa Barbara, CA: Nat. Center Geographic Inf. Anal., 2002.

Buermann, W., P. R. Bikash, M. Jung, D. H. Burn, and M. Reichstein. (2013). Earlier springs decrease peak summer productivity in North American boreal forest. *Environmental Research Letters*, 8, 024027

Chang, A. T. C., J. L. Foster, and D. K. Hall. (1990). Satellite sensor estimates of northern hemisphere snow volume. *International Journal of Remote Sensing*, 11 (1), 167-171

Colliander, A., K. C. McDonald, R. Zimmermann, R. Schroeder, J. S. Kimball, and E. G. Njoku. (2012). Application of QuikSCAT backscatter to SMAP validation planning: Freeze/Thaw state over ALECTRA sites in Alaska from 2000 to 2007. *IEEE Transactions on Geoscience and Remote Sensing*, 50 (2), 461-468

Dee, D. P., S. M. Uppala, A. J. Simmons, P. Berrisford, P. Poli, S. Kobayashi, U. Andrae, M. A. Balmasewda, G. Balsamo, P. Bauer, P. Bechtold, A. C. M. Beljaars, L. van de Berg, J. Bidlot, N. Bormann, C. Delsol, R. Dragani, M. Fuentes, A. J. Geer, L. Haimberger, S. B. Healy, H. Hersbach, E. V. Holm, L. Isaksen, P. Kallberg, M. Kohler, M. Matricardi, A. P. McNally, B. M. Monge-Sanz, J. J. Morcrette, B. K. Park, C. Peubey, P. de Rosnay, C. Tavolato, J. N. Thepaut, and F. Vitart. (2011). The ERA-Interim reanalysis: configuration and performance of the data assimilation system. *Quarterly Journal of the Royal Meteorological Society*, 137, 553-597

Earth Syst. Sci. Data Discuss., doi:10.5194/essd-2016-27, 2016
Manuscript under review for journal Earth Syst. Sci. Data
Published: 22 July 2016

Dendoncker, N., C. Schmit, and M. Rounsevell. (2013). Exploring spatial data uncertainties in land-use change scenarios. *International Journal of Geographical Information Science*, 22:9, 1013-1030

de Jong, R., M. E. Schaepman, R. Furrer, S. de Bruin, and P. H. Verburg. (2013). Spatial relationship between climatologies and changes in global vegetation activity. *Global Change Biology*, 19, 1953-1964

Defourny, P.; Kirches, G.; Brockmann, C.; Boettcher, M.; Peters, M.; Bontemps, S.;Lamarche, C.; Schlerf, M.; Santoro, M. (2016). Land Cover CCI: Product User Guide Version 2. Available online: http://maps.elie.ucl.ac.be/CCI/viewer/download/ESACCI-LC-PUG-v2.5.pdf

Derksen, C., A. Walker, and B. Goodison. (2005). Evaluation of passive microwave snow water equivalent retrievals across the boreal forest/tundra transition of western Canada. *Remote Sensing of Environment*, 96, 315-327

Du, J., J. S. Kimball, M. Azarderakhsh, R. S. Dunbar, M. Moghaddam, and K. C. McDonald. (2015). Classification of Alaska spring thaw characteristics using L-band radar remote sensing. *IEEE Transactions on Geoscience and Remote Sensing*, 53 (1), 542-556

Ferraro, R. R., F. Weng, N. C. Grody, and A. Basist. (1996). An eight-year (1987–1994) time series of rainfall, clouds, water vapor, snow cover, and sea ice derived from SSM/I measurements. *Bulletin of the American Meteorological Society*, 77 (5), 891–905.

Friedl, M. A., D. Sulla-Menashe, B. Tan, A. Schneider, N. Ramankutty, A. Sibley, and X. Huang. (2010). MODIS Collection 5 global land cover: Algorithm refinements and characterization of new datasets. *Remote Sensing of Environment*, 114, 168-182

Frolking, S., K. C. McDonald, J. S. Kimball, J. B. Way, R. Zimmermann, and S. W. Running. (1999). Using the space-borne NASA scatterometer (NSCAT) to determine the frozen and thawed seasons. *Journal of Geophysical Research*, 104 (D22), 27895-27907

Green, J. C. Kongoli, A. Prakash, M. Sturm, C. Duguay, and S. Li. (2012). Quantifying the relationships between lake fraction, snow water equivalent and snow depth, and microwave brightness temperatures in an arctic tundra landscape. *Remote Sensing of Environment*, 127, 329-340

Grody, N. C., and A. N. Basist. (1996). Global Identification of snowcover using SSM/I measurements. *Transactions on Geoscience and Remote Sensing*, 34 (1), 237-249

Hakkinen, S., D. K. Hall, C. A. Shuman, D. L. Worthen, and N. E. DiGirolamo. (2014). Greenland ice sheet melt from MODIS and associated atmospheric variability. *Geophysical Research Letters*, 41, 1600-1607

Earth Syst. Sci. Data Discuss., doi:10.5194/essd-2016-27, 2016
Manuscript under review for journal Earth Syst. Sci. Data
Published: 22 July 2016

Han, M., K. Yang, J. Qun, R. Jin, Y. Ma, J. Wen, Y. Chen, L. Zhao, L. Zhu, and W. Tang. (2015). An Algorithm based on the standard deviation of passive microwave brightness temperatures for monitoring soil surface freeze/thaw state on the Tibetan Plateau. *IEEE Transactions on Geoscience and Remote Sensing*, 53 (5), 2775-2783

Hasting, D. A., P. K. Dunbar, G. M. Elphingstone, M. Bootz, H. Murakami, H. Maruyama, H. Masaharu, P. Holland, J. Payne, N. A. Bryant, T. L. Logan, J.-P. Muller, G. Schreier, and J. S. MacDonald, GLOBE Task Team. (1999). The global land one kilometer base elevation (GLOBE) digital elevation model, version 1.0, Nat. Ocean. Atmos. Admin., Nat. Geophys. Data Center, Boulder, CO, Digital data base on the World Wide Web and CD-ROMs. [Online]. Available: http://www.ngdc.noaa.gov/mgg/toto/globe.html

Holmes, T. R. H., W. T. Crow, M. T. Yilmaz, T. J. Jackson, and J. B. Basara. (2013). Enhancing model-based land surface temperature estimates using multiplatform microwave observations. *Journal of Geophysical Research: Atmosphere*, 118, 577-591

Howell, S. E. L., L. C. Brown, K. Kang, and C. R. Duguay. (2009). Variability in ice phenology on Great Bear Lake and Great Salve lake, northwest territories, Canada, from SeaWinds/QuikSCAT: 2000-2006. *Remote Sensing of Environment*, 113, 816-834

Kenney, M. A., A. C. Janetos, et al., (2014). National Climate Indicators System Report, National Climate Assessment and Development Advisory Committee. Available online: http://www.globalchange.gov/sites/globalchange/files/Pilot-Indicator-System-Report_final.pdf (accessed on 11 May 2016)

Kim, Y., J. S. Kimball, D. A. Robinson, and C. Derksen. (2015). New satellite climate data records indicate strong coupling between recent frozen season changes and snow cover over high northern latitudes. *Environmental Research Letters*, 10, 084004.

Kim, Y., J. S. Kimball, K. Zhang, K. Didan, I. Velicogna, and K. C. McDonald (2014a). Attribution of divergent northern vegetation growth responses to lengthening non-frozen seasons using satellite optical-NIR and microwave remote sensing, *International Journal of Remote Sensing*, 10.1080/01431161.2014.915595

Kim, Y., J. S. Kimball, K. Didan, and G. M. Henebry. (2014b). Responses of vegetation growth and productivity to spring climate indicators in the conterminous Unites States derived from satellite remote sensing data fusion. *Agricultural and Forest Meteorology*, 194, 132-143

Kim, Y., J. S. Kimball, J. Glassy, and K. C. McDonald (2014c). MEaSUREs Global Record of Daily Landscape Freeze/Thaw Status. Version 3. [1979-2011]. Boulder, Colorado USA: NASA DAAC at the National Snow and Ice Data Center. http://dx.doi.org/10.5067/MEASURES/CRYOSPHERE/nsidc-0477.003

Earth Syst. Sci. Data Discuss., doi:10.5194/essd-2016-27, 2016
Manuscript under review for journal Earth Syst. Sci. Data
Published: 22 July 2016

Kim, Y., J. S. Kimball, K. Zhang, and K. C. McDonald (2012). Satellite detection of increasing northern hemisphere non-frozen seasons from 1979 to 2008: Implications for Regional Vegetation Growth. *Remote Sensing of Environment*, 121, 472-487

Kim, Y., J. S. Kimball, K. C. McDonald, and J. Glassy (2011). Developing a global data record of daily landscape freeze/thaw status using satellite passive microwave remote sensing. *IEEE Transactions on Geoscience and Remote Sensing*, 49 (3), 949-960

Kimball, J. S., K. C. McDonald, A. R. Keyser, S. Frolking, and S. W. Running. (2001). Application of the NASA scatterometer (NSCAT) for determining the daily frozen and nonfrozen landscape of Alaska. *Remote Sensing of Environment*, 75, 113-126

Knowles, K. (2004). EASE-Grid Land-Ocean-Coastline-Ice Masks Derived from Boston University MODIS/Terra Land Cover Data. [indicate subset used]. Boulder, Colorado USA: NASA National Snow and Ice Data Center Distributed Active Archive Center. http://dx.doi.org/10.5067/YR21Q0Q8IPR6

Knowles, K., E.G. Njoku, R. Armstrong, and M. Brodzik. (2000). Nimbus-7 SMMR Pathfinder Daily EASE-Grid Brightness Temperatures [1979-1987]. Boulder, Colorado USA: NASA DAAC at the National Snow and Ice Data Center (http://nsidc.org/data/nsidc-0071.html).

Lemmetyinen, J., A. Kontu, J. Karna, J. Vehvilainen, M. Takala, and J. Pulliainen. (2011). Correcting of the influence through application of a microwave emission model. *Remote Sensing of Environment*, 115, 3965-3706

Mao, J., W. Fu, X. Shi, D. M. Ricciuto, J. B. Fisher, R. E. Dickinson, Y. Wei, W. Shem, S. Piao, K. Wang, C. R. Schwalm, H. Tian, M. Mu, A. Arain, P. Ciais, R. Cook, Y. Dai, D. Hayes, F. M. Hoffman, M. Huang, S. Huang, D. N. Huntzinger, A. Ito, A. Jain, A. W. King, H. Lei, C. Lu, A. M. Michalak, N. Parazoo, C. Peng, S. Peng, B. Poulter, K. Schaefer, E. Jafarov, P. E. Thornton, W. Wang, N. Zeng, Z. Zeng, F. Zhao, Q. Zhu, and Z. Zhu. (2015). Disentangling climate and anthropogenic controls on global terrestrial evaporation trends. *Environmental Research Letters*, 10, 094008

Matzler, C. (1994). Passive microwave signatures of landscapes in Winter. *Meteorology and Atmospheric Physics*, 54, 241-260

Mote, T. L. (2014). MEaSUREs Greenland Surface Melt Daily 25km EASE-Grid 2.0. [indicate subset used]. Boulder, Colorado USA: NASA National Snow and Ice Data Center Distributed Active Archive Center. http://dx.doi.org/10.5067/MEASURES/CRYOSPHERE/nsidc-0533.001

Naeimi, V., C. Paulik, A. Bartsch, W. Wagner, R. Kidd, S. Park, K. Elger, and J. Bioke. (2012). ASCAT surface state flag (SSF): extracting information on surface freeze/thaw conditions from backscatter data using an empirical threshold-analysis algorithm. *IEEE Transactions on Geoscience and Remote Sensing*, 50 (7), 2566-2582

Nenana Ice Classic. (2011). Nenana Ice Classic: Tanana River Ice Annual Breakup Dates. [indicate subset used]. Boulder, Colorado USA: National Snow and Ice Data Center. http://dx.doi.org/10.5067/DURFYP131STS

Earth Syst. Sci. Data Discuss., doi:10.5194/essd-2016-27, 2016
Manuscript under review for journal Earth Syst. Sci. Data
Published: 22 July 2016

Nghiem, S. V., D. K. Hall, T. L. Mote, M. Tedesco, M. R. Albert, K. Keegan, C. A. Shuman, N. E. DiGirolamo, and G. Neumann. (2012). The extreme melt across the Greenland ice sheet in 2012. *Geophysical Research Letters*, 39, L20502

National Weather Services (NWS). (1988). Surface Observations, Federal Meteorological Handbook no. 1 (FCM-H1-1988), Washington, DC: Dept. Commerce, Office Federal Coordinator 1988.

Owe, M., R. de Jeu, and T. Holmes. (2008). Multisensor historical climatology of satellite-derived global land surface moisture. *Journal of Geophysical Research*, 113, F01002

Owe, M., and A. A. Van De Griend. (2001). On the relationship between thermodynamic surface temperature and high-frequency (37 GHz) vertically polarized brightness temperature under semi-arid conditions. International Journal of Remote Sensing, 22 (17), 3521-3532

Park, H., Y. Kim, and J. S. Kimball. (2016a). Widespread permafrost vulnerability and soil active layer increases over the high northern latitudes inferred from satellite remote sensing and process model assessments. *Remote Sensing of Environment*, 175, 349-358

Park, H., Y., Yoshikawa, K. Oshima, Y. Kim, T. Ngo-Duc, and J. S. Kimball, and D. Yang. (2016b). Quantification of warming climate-induced changes in terrestrial arctic river ice thickness and phenology. *Journal of Climate*, 29, 1733-1754

Peterson, T. C. (2005). Climate Change Indices. WMO *Bulletin*, 54 (2), 83-86

Podest, E., K. C., McDonald, & J. S. Kimball. (2014). Multisensor microwave sensitivity to freeze/thaw dynamics across a complex boreal landscape. *IEEE Transactions on Geoscience and Remote Sensing*, 52 (11), 6818-6828

Prigent, C., F. Aires, and W. B. Rossow. (2006). Land surface microwave emissivities over the globe for a decade. *Bulletin of the American Meteorological Society*, 87, 1573-1584

Rautiainen, K., J. Lemmetyinen, M. Schwank, A. Kontu, C. B. Menard, C. Matzler, M. Drusch, A. Wiesmann, J. Ikonen, and J. Pulliainen. (2014). Detection of soil freezing from L-band passive microwave observations. *Remote Sensing of Environment*, 147, 206-218

Rawlins, M. A., K. C. McDonald, S. Frolking, R. B. Lammers, M. Fahnestock, J. S. Kimball, and C. J. Vorosmarty. (2005). Remote sensing of snow thaw at the pan-Arctic scale using the SeaWinds scatterometer. *Journal of Hydrology*, 312, 294-311

Rees, A., C. Derksen, M. English, A. Walker, and C. Duguay. (2006). Uncertainty in snow mass retrievals from satellite passive microwave data in lake-rich high-latitude environments. *Hydrological Processes*, 20, 1019-1022

Screen, J. A, C. Deser, and I. Simmonds. (2012). Local and remote controls on observed Arctic warming. *Geophysical Research Letters*, 39, L10709

Earth Syst. Sci. Data Discuss., doi:10.5194/essd-2016-27, 2016
Manuscript under review for journal Earth Syst. Sci. Data
Published: 22 July 2016

Ulaby, F. and D.G. Long. (2014). Microwave Radar and Radiometric Remote Sensing, University of Michigan Press, Ann Arbor, Michigan

Wang, X., S. Piao, X. Xu, P. Ciais, N. MacBean, R. B. Myneni and L. Li. (2015). Has the advancing onset of spring vegetation green-up slowed down or changed abruptly over the last three decades?. *Global Ecology and Biogeography*, 24, 621-631

Zhang, S., X. Li, Y. Ma, G. Zhao, L. Li, J. Chen, Z. Jiang, and Y. Huang. (2014). Interannual and seasonal variability in evapotranspiration and energy partitioning over the alpine riparian shrub Myricaria squamosal Desv. On Qinghai-Tibet Plateau. *Cold Regions and Science and Technology*, 102, 8-20

Zhang, K., J. S. Kimball, Y. Kim, & K. C. McDonald. (2011). Changing freeze-thaw seasons in northern high latitudes and associated influences on evapotranspiration. *Hydrological Processes*, 25, 4142-4151

Zhao, M., J. Ramage, K. Semmens, and F. Obleitner. (2014). Recent ice cap snowmelt in Russian High Arctic and anti-correlation with late summer sea ice extent. *Environmental Research Letters*, 9, 045009

Zhu, Z., S. Piao, R. B. Myneni, M. Huang, Z. Zeng, J. G. Canadell, P. Ciais, S. Stich, P. Friedlingstein, A. Arneth, C. Cao, L. Cheng, E. Kato, C. Koven, Y. Li, X. Lian, Y. Liu, R. Liu, J. Mao, Y. Pan, S. Peng, J. Penuelas, B. Poulter, T. A. M. Pugh, B. D. Stocker, N. Viovy, X. Wang, Y. Wang, Z. Xiao, H. Yang, S. Zaehle, and N. Zeng. (2016). Greening of the Earth and its drivers. *Nature Climate Change*, doi:10.1038/nclimate3004

Earth Syst. Sci. Data Discuss., doi:10.5194/essd-2016-27, 2016
Manuscript under review for journal Earth Syst. Sci. Data
Published: 22 July 2016

Table 1. Mean monthly FT classification agreement (%) for AM and PM overpasses in relation to WMO surface air temperature (SAT_{max} and SAT_{min}) based FT metrics for Northern Hemisphere (NH), Southern Hemisphere (SH) and global domains. Values represent mean monthly spatial agreement (%) and temporal standard deviation for the 1979–2014 record.

	PM overpass			AM overpass		
	NH	SH	Global	NH	SH	Global
Jan	81.0±1.9	96.3±1.8	81.9±2.0	80.0±1.6	95.8±2.0	80.9±1.7
Feb	81.9±1.8	96.8±1.7	82.7±1.9	80.7±1.6	96.5±1.5	81.6±1.6
Mar	84.3±2.5	96.5±1.6	84.9±2.5	78.9±2.0	95.4±1.1	79.8±2.1
Apr	91.6±1.8	96.1±1.4	91.9±1.9	77.8±2.4	92.5±2.1	78.6±2.5
May	96.0±0.9	96.0±1.4	96.0±1.0	86.3±2.7	87.0±2.8	86.3±2.6
Jun	97.6±0.7	94.8±1.9	97.5±0.7	94.8±1.9	80.1±3.9	94.0±1.7
Jul	98.1±0.5	93.7±2.3	97.9±0.5	97.0±1.2	77.2±3.0	95.9±0.9
Aug	97.5±0.6	94.1±2.0	97.3±0.6	96.0±1.3	80.6±2.9	95.1±1.1
Sep	96.1±0.8	95.3±1.7	96.1±0.8	89.2±2.4	86.2±2.9	89.0±2.3
Oct	91.4±1.9	96.0±1.4	91.6±1.9	77.5±3.2	91.1±1.6	78.3±3.3
Nov	83.5±2.7	96.1±1.7	84.2±2.8	73.7±2.3	93.5±1.5	74.9±2.5
Dec	80.2±1.9	96.0±3.0	81.1±2.0	76.3±2.2	94.7±1.7	77.4±2.3

Earth Syst. Sci. Data Discuss., doi:10.5194/essd-2016-27, 2016
Manuscript under review for journal Earth Syst. Sci. Data
Published: 22 July 2016

Table 2. Mean annual FT-ESDR PM overpass spatial agreement (%) with WMO station based FT metrics by dominant IGBP land cover class for 2012. Values represent mean and one spatial standard deviation variability in relative spatial accuracy, while the number of weather stations used for FT accuracy assessment within each land cover category is also noted.

*Land cover class	PM overpass	AM overpass	Number of stations
Water	77.5±18.3	75.0±15.4	536
ENF	88.6±6.5	84.5±6.3	202
EBF	98.6±4.3	88.4±14.8	38
DNF	93.5±5.7	89.3±4.7	32
DBF	96.2±3.1	88.0±4.0	84
MF	93.1±7.0	86.7±6.7	751
OS	95.8±5.9	89.9±7.2	345
WS	96.2±5.9	92.1±5.9	381
SVM	99.1±2.6	96.1±4.9	19
GRS	92.9±7.5	87.7±6.9	888
PW	91.4±6.2	86.4±4.9	8
CL	94.9±5.7	88.8±5.7	1286
Urban	96.5±3.9	89.5±4.6	102
CL/NVM	94.4±4.5	87.2±4.4	559
Snow/ice	81.1±19.6	83.1±21.3	30
Barren	94.3±6.5	91.8±4.5	82

*Land cover classes represented include open water (Water), evergreen needleleaf forest (ENF), evergreen broadleaf forest (EBF), deciduous needleleaf forest (DNF), deciduous broadleaf forest (DBF), mixed forest (MF), open shrubland (OS), woody savanna (WS), savanna (SVN), grassland (GRS), permanent wetland (PW), cropland (CL), urban (Urban), cropland/natural vegetation mosaic (CL/NVM), permanent snow/ice (Snow/ice) and barren or sparsely vegetation (Barren) categories. Closed shrubland is excluded in this analysis because only a single CS station was identified.

Earth Syst. Sci. Data Discuss., doi:10.5194/essd-2016-27, 2016
Manuscript under review for journal Earth Syst. Sci. Data
Published: 22 July 2016

Open Access Earth System Science Data Discussions

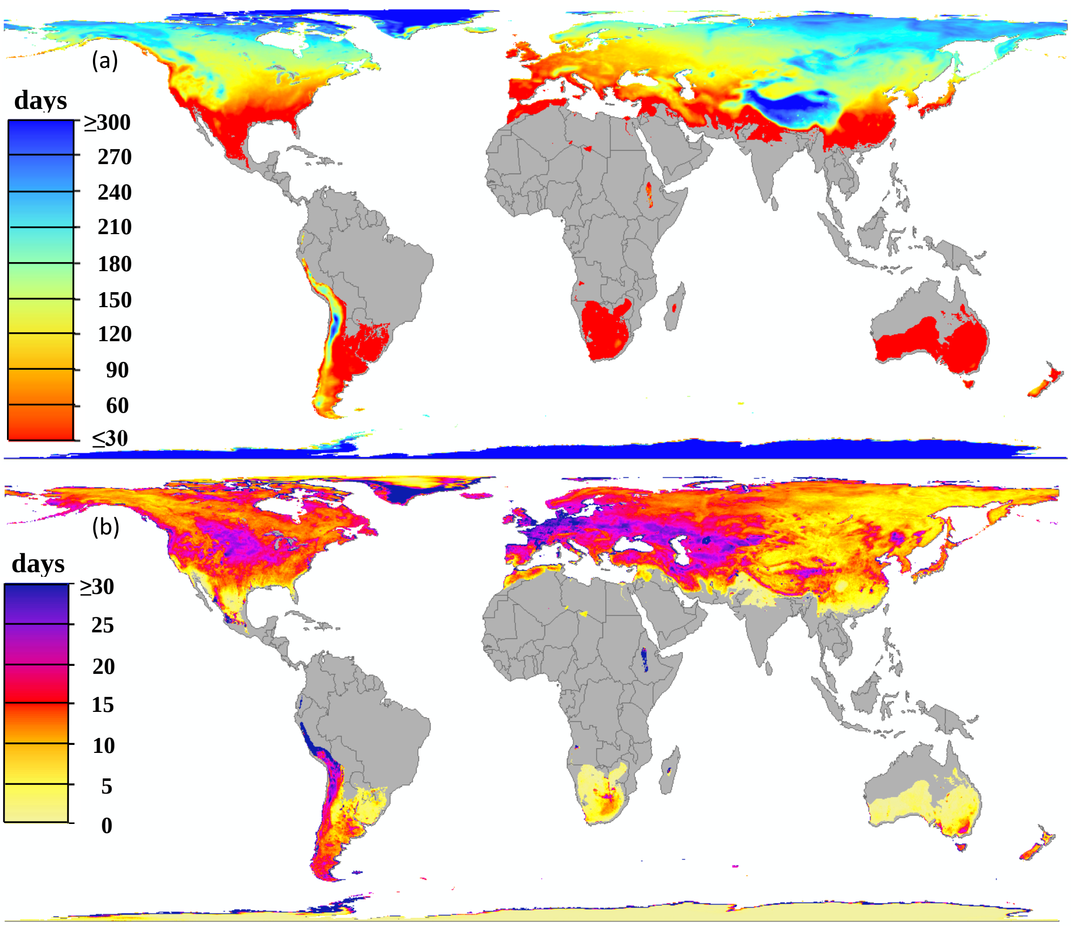

Figure 1. (a) Mean annual frozen season (frozen or transitional status) and (b) standard deviation of the frozen season over the 36-year (1979-2014) record and Global FT-ESDR domain; white and grey colors denote respective open water bodies and land areas outside of the FT-ESDR domain; grey areas depict grid cells where the mean cold temperature constraint index (CCI) was less than 5 days yr^{-1} from the 36-year CCI record.

Earth Syst. Sci. Data Discuss., doi:10.5194/essd-2016-27, 2016
Manuscript under review for journal Earth Syst. Sci. Data
Published: 22 July 2016

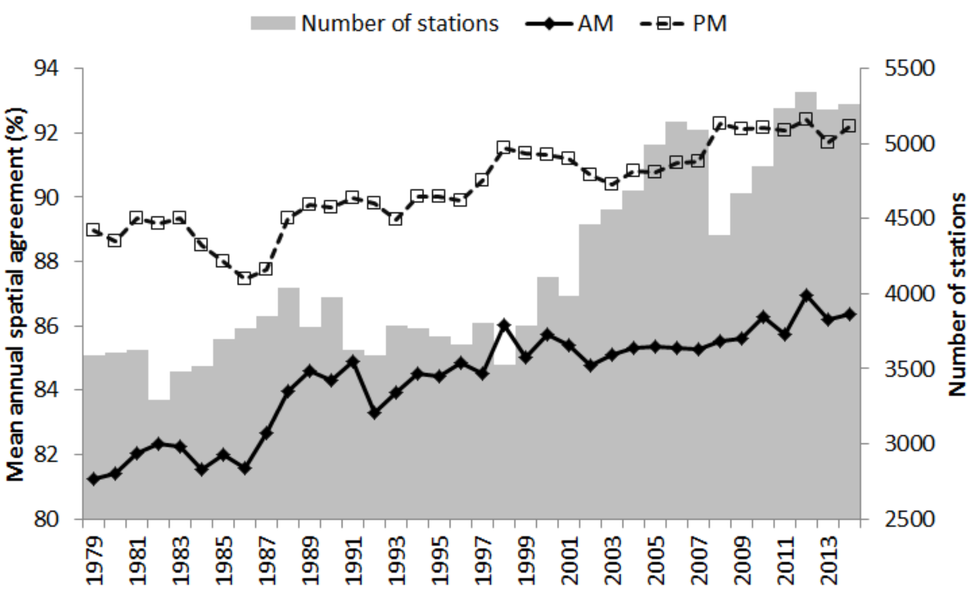

Figure 2. Mean annual FT spatial classification agreement (%) between FT-ESDR results and corresponding daily SAT based FT estimates from the global WMO weather station network. The FT classification agreement was determined on a daily basis for individual satellite AM and PM overpasses in relation to grid cell-to-point comparisons with independent FT estimates derived from respective minimum and maximum daily SAT records. The bar graph denotes the number of global WMO stations used for FT assessment.

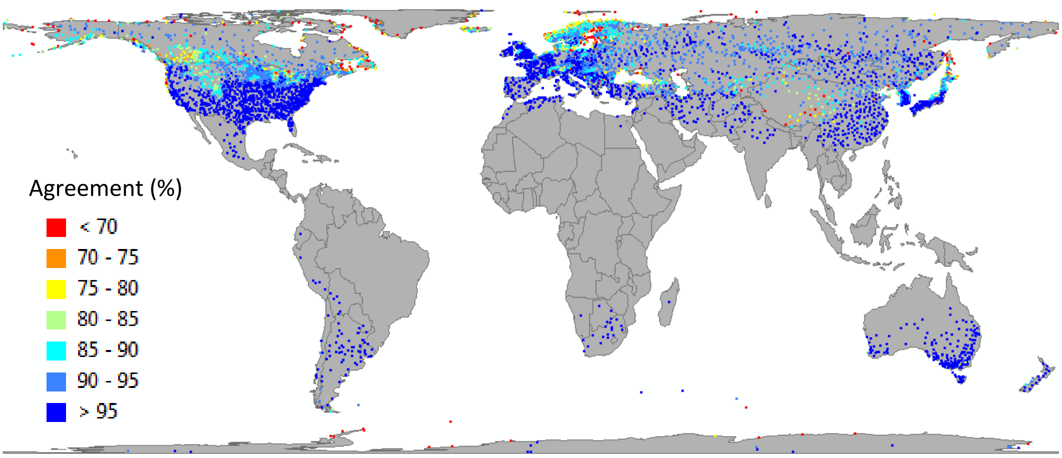

Figure 3. Spatial distribution of mean annual FT classification agreement (%) for PM overpass results in relation to grid cell-to-point comparisons with 5344 WMO station SAT_{max} based FT observation locations for 2012.

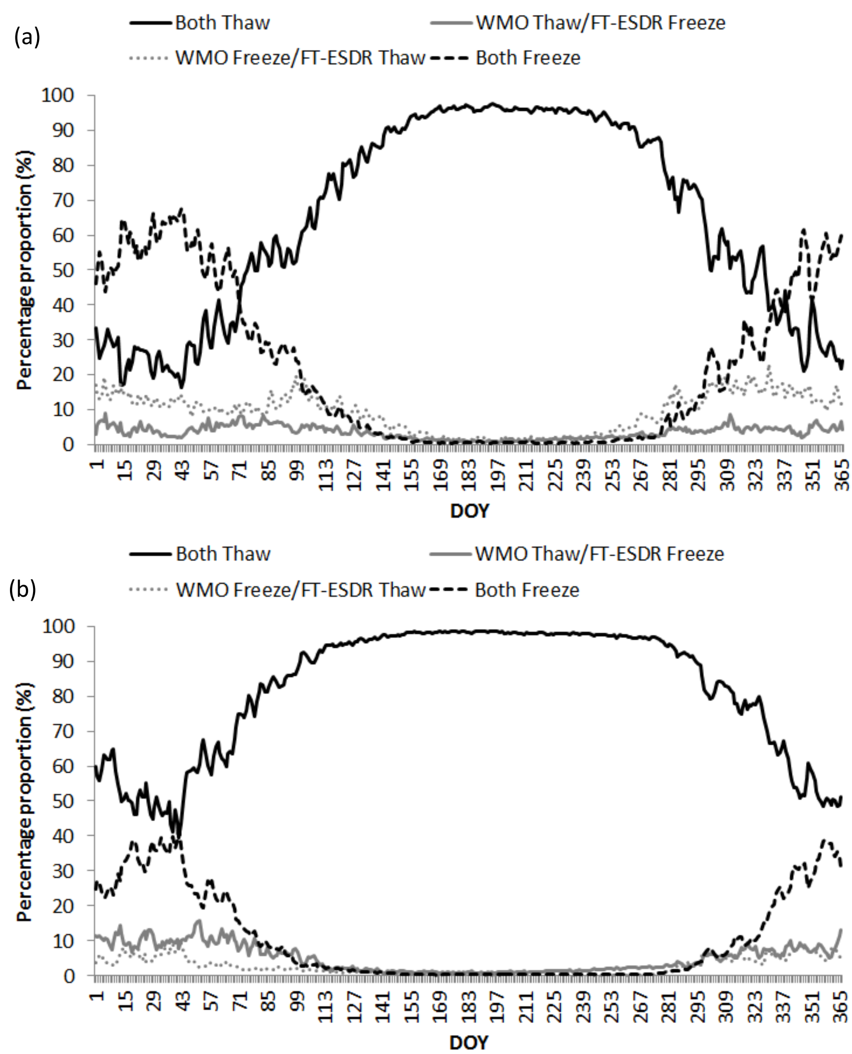

Figure 4. Seasonal pattern of proportional (%) agreement and disagreement derived from grid cell-to-point comparisons between 5344 WMO surface air temperature (SAT_{min} and SAT_{max}) derived FT values and the corresponding AM and PM FT-ESDR for 2012: (a) SAT_{min} and AM overpass; (b) SAT_{max} and PM overpass.

Earth Syst. Sci. Data Discuss., doi:10.5194/essd-2016-27, 2016
Manuscript under review for journal Earth Syst. Sci. Data
Published: 22 July 2016

Open Access Earth System Science Data Discussions

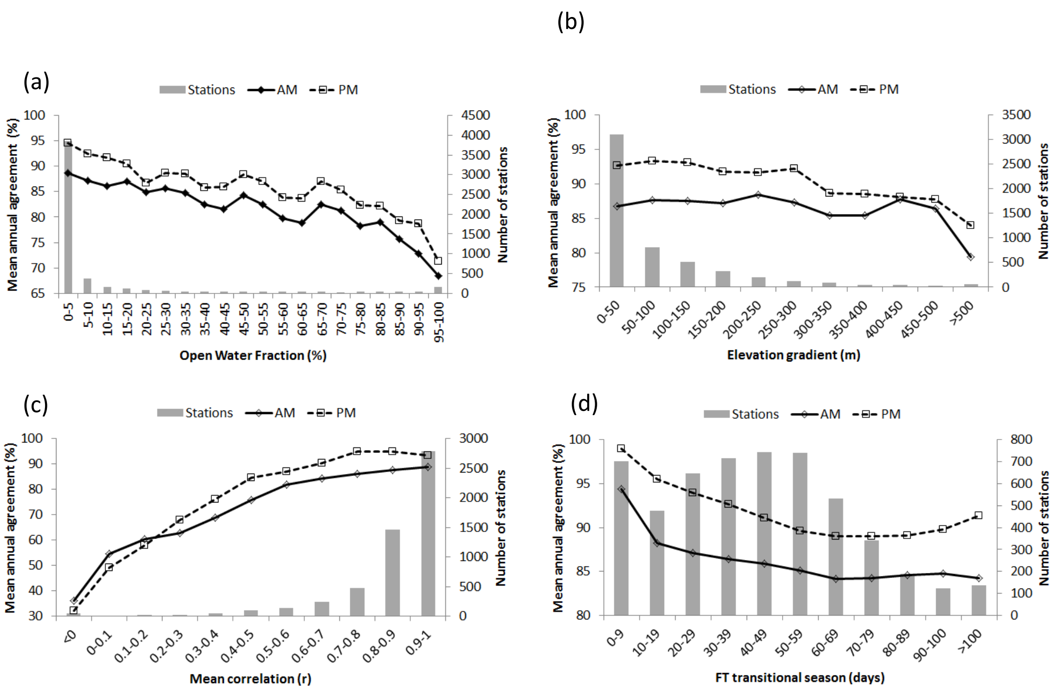

Figure 5. Dominant factors affecting AM and PM overpass FT classification agreement for individual grid cells, including: (a) open water fraction within a grid cell (F_w, %); (b) terrain elevation gradient (m) within a cell; (c) correlation (r-value) of grid cell linear regression relationship between satellite T_b retrievals and weighted ERA-Interim SAT used in determining the MSTA FT threshold, and (d) the annual FT transitional season duration (days).

Earth Syst. Sci. Data Discuss., doi:10.5194/essd-2016-27, 2016
Manuscript under review for journal Earth Syst. Sci. Data
Published: 22 July 2016

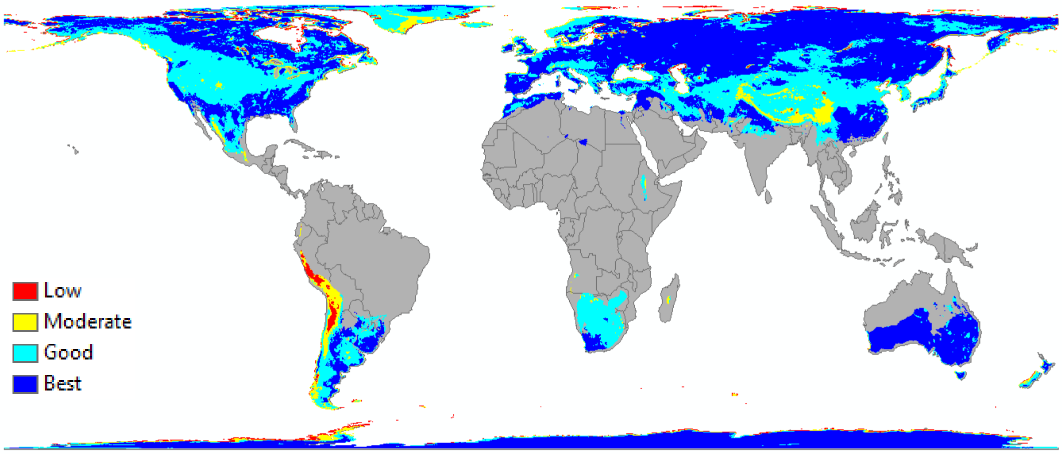

Figure 6. FT-ESDR annual quality assurance (QA) map for 2012, aggregated into low (estimated mean annual spatial classification agreement < 70%), moderate (75-85%), good (85-95%) and best (>95%) relative quality categories. Land areas outside of the FT-ESDR domain are denoted by grey shading; grey shadings depict grid cells where the mean cold temperature constraint index (CCI) was less than 5 days yr^{-1} from the 36-year CCI record.

Earth Syst. Sci. Data Discuss., doi:10.5194/essd-2016-27, 2016
Manuscript under review for journal Earth Syst. Sci. Data
Published: 22 July 2016

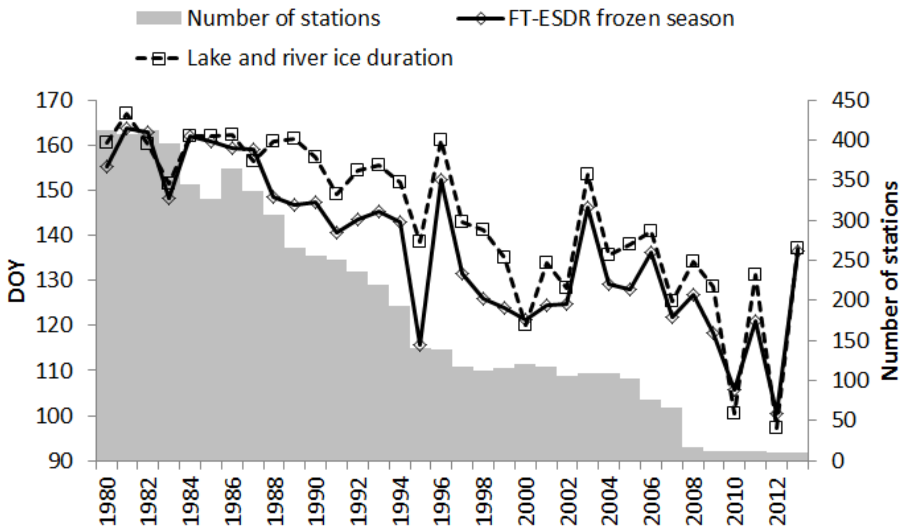

Figure 7. Correspondence between mean annual (1979-2013) lake ice duration observations for lake and river ice and FT-ESDR derived frozen season (frozen or transitional status).

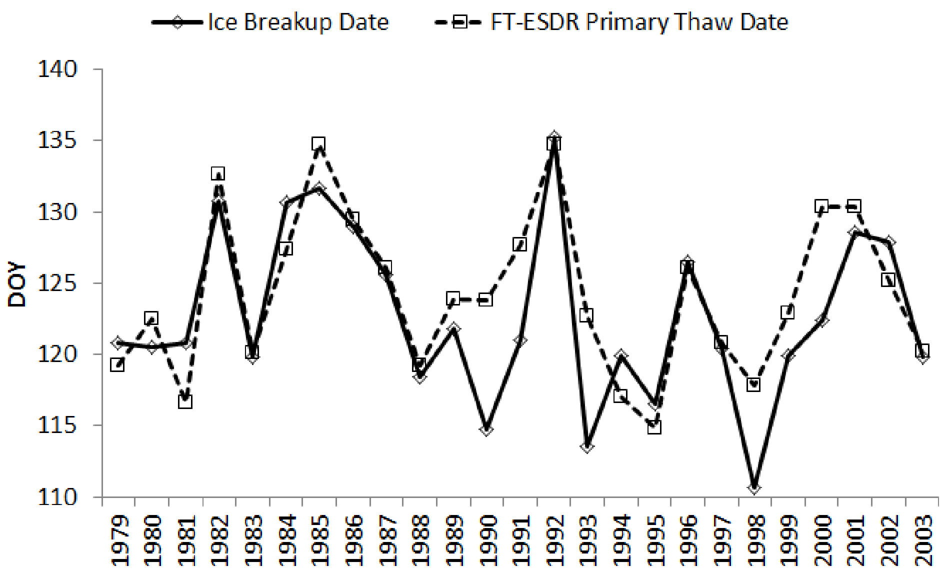

Figure 8. Correspondence between reported annual ice breakup dates for the Tanana River, AK (64.56°N, 140.09°W) and FT-ESDR derived primary spring thaw onset averaged within a 5x5 grid cell (~125x125km) window overlying the basin.

Earth Syst. Sci. Data Discuss., doi:10.5194/essd-2016-27, 2016
Manuscript under review for journal Earth Syst. Sci. Data
Published: 22 July 2016

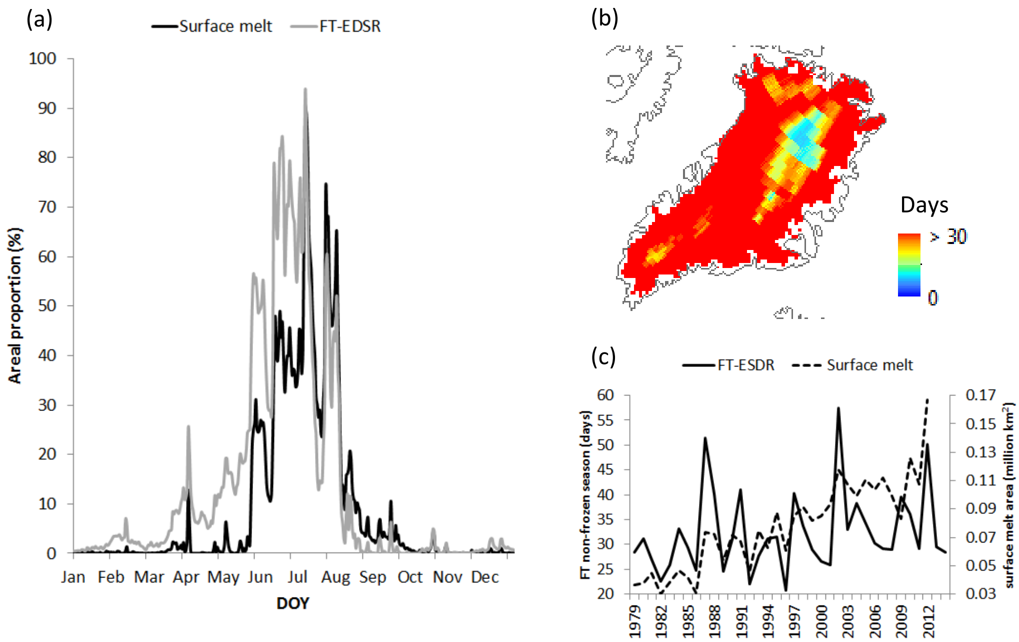

Figure 9. Seasonal progression in proportional area of surface melt (Mote, 2014) and FT-ESDR derived non-frozen conditions over the Greenland ice sheet in 2012 (a). The spatial pattern of the FT-ESDR derived annual non-frozen season (days) over the Greenland ice sheet is also shown (b). Annual variations in annual surface melt area and non-frozen season over the 36-year FT-ESDR record are also presented (c); these results document a general increase in the non-frozen season (1.7 days decade^{-1}; p=0.2) that coincides with increasing surface melt (0.03 million km^2 decade^{-1}; p<0.001) over Greenland and a 0.6°C decade^{-1} (p<0.01) regional SAT warming trend indicated from ERA-Interim reanalysis.